*Proceedings IRF2018: 6th International Conference Integrity-Reliability-Failure*
*Lisbon/Portugal 22-26 July 2018. Editors J.F. Silva Gomes and S.A. Meguid*
*Publ. INEGI/FEUP (2018); ISBN: 978-989-20-8313-1*

PAPER REF: 7132

# STUDY OF A CRASH BOX DESIGN OPTIMIZED FOR A UNIFORM LOAD PROFILE

**A. Segade[1(*)], A. Bolaño[1], J.A. López-Campos[1], E. Casarejos[1], J.R. Fernandez[2], J.A. Vilán[1]**
[1]Department of Mechanical Engineering, University of Vigo, E-36310 Vigo, Spain
[2]Department of Applied Mathematics I, University of Vigo, E-36310 Vigo, Spain
[(*)]*Email:* asegade@uvigo.es

## ABSTRACT

The interest for more efficient safety systems for the automotive market includes multiple mechanical parts. One of the key systems for the energy absorption in an impact situation is the front-rail, including the so-called crash boxes. Designed for low speed impacts, the purpose of this box is to deform by crushing, causing a characteristic load transmission to the vehicle. The possibility to design the boxes to avoid extreme load (acceleration) peaks is an opportunity to improve the overall safety of the vehicle. We study a feasible option to design the pre-deformation of the boxes according to the buckling shape modes. The analysis of the mode shapes can guide the selection of the more efficient cases. The comparative study of the load patterns induced by the different options can provide the most appropriate shape to reduce the load peaks. We focus in squared sections, and also compared the effects of wall thickness and material stiffness. We analyse further the implementation to a realistic crash-box plus bumper system. We also propose a series box mounting to study the possibility to design systems capable to distribute the energy absorption in quasi-independent stages according to the energy levels. We study a case of section and size defined and a reduced set of materials, however the method allows for more detailed studies to analyse solutions to specific situations.

***Keywords:*** crashworthiness, LS-DYNA, ANSYS, impact, crash box, buckling

## 1. INTRODUCTION

The better understanding of the materials properties and the behaviour of structures under impact conditions, drives continuous improvements in the safety systems dedicated to the automotive industry. In modern cars up to 50% of the impact energy may be absorbed by the front-rail structure (Witteman, 1999) in front impact situations. The right understanding of these parts started with the studies dedicated to axial crushing developed in the 80's (Gao, 1984; Abramazovick, 1984). Most of the works were based in structures with uniform cross-sections in the length (Yamazaki, 1998; Abramovizc, 1986), and described the irregular load pattern caused by the folding and crushing of the structure during the crushing process.

These studies also allowed for early proposals (Mamalis, 1986; Grzebieta, 1985; Grzebieta, 1986) to smooth the impact load patterns by modifying the structure profiles with deformation triggers. An efficient and simple method to make triggers in structures is with drills (Arnold, 2004; Mamalis, 2009). Other methods proposed combine efficiency with feasibility, including (axisimmetric) circumferential grooves (Hosseinipour, 2003; Acar, 2011) and transversal dents (Lee, 1999; Asanjarani, 2017). A review is given by (Yuen, 2008). A different option is

to find an optimal geometry to improve the energy absorption although this method implies the use of complex geometries. This is the option followed by Tanlak to find an optimal shape of a bumper beam (Tanlak, 2015) or for a thin-walled tube under axial impact (Tanlak, 2014).

The new concepts allowed improving the energy absorption in vehicles for both conventional models (Kokkula, 2006) and new growing markets, as for heavy quadricycles (Lopez-Campos, 2015). This work studies the performance of complex geometries of the crash box part of an energy absorption system, still feasible for industrial implementation. The geometry is based in the (static) buckling modes of the structure. This strategy has been studied by (Langseth, 1994) analysing the better performance of these structures in dynamic conditions. There was also a proposal by (Abramowicz, 1997) to relate the static buckling (according to Euler formulation) with the start of the dynamical buckling, just limited to the basic modes. Some studies proposed using an eigenvalue buckling analysis before the dynamical nonlinear crushing evaluation for considering the geometrical imperfections (Nagel, 2006). In this work we extend the study to multiple modes and establish a selection rule for the interesting modes to make a study of the more convenient deformation to improve the load profile.

The paper is outlined as follows. In section 2 we present the case study and discuss the selection of the proper eigenvalue buckling modes for the following analysis. In section 3 we define the dynamical test performed. In section 4 we analyse the results provided by the different modes and deformation scaling, to discuss the best option. In sections 5 and 6 we study the influence of wall thickness and material selection. In the last section we analyse the implementation of the selected crash-box into a bumper system and propose a double serial crash-box system to study the energy absorption capabilities.

## 2. BUCKLING MODES

The buckling deformation of a crash-box under a certain load is governed by the geometrical imperfections of the structure, material in-homogeneities and residual stresses after the welding, extruding, plying, etc. of the part. Typically just before an unknown buckling pattern triggers under a pressure load is applied, there is a hardening effect due to the instability caused, inducing a fast load increase (Albert, 2016). During the plying of a buckling shape the load decreases, and only when the plies make a new material contact, the compression load increases again and, maybe, causing new buckling plies. This process generates peaks and oscillation of the loads between minimum and maximum values (Langseth, 1999).

To have a better control on the load pattern, and for being predictable, it is possible to tune the structure geometry so that the weak points are pre-defined. One option is to pre-deform the shape of the structure according the (static) buckling mode shapes. Under these conditions, the load applied is used to deform the structure following a deformation pattern designed to improve the load profile from the safety point of view.

### 2.1 The analysis of buckling modes in FE models

The finite element (FE) method to solve the linear buckling is based in the matrix equation

$$([K] + N[K_{geo}])\{d\} = \{F\}$$

where [K] is the stiffness matrix, {d} the displacement vector of the mesh points, {F} the load vector and N the axial load. $[K_{geo}]$ is the 'geometric' stiffness matrix obtained from the integration of the element shape functions. It is related to the geometrical non-linearity of the

structure studied (Cook, 1974). The buckling conditions happen when [K] is small and therefore tiny perturbations cause large displacements. The problem then reduces to solve the eigenvalues N that cause the singularity of the matrix [K]

$$\det ( [K] + N[K_{geo} ] ) = 0$$

The N values correspond to the axial loads that cause the buckling, and the corresponding eigenvectors are the mode shapes for buckling. The modes can be extracted for post-buckling analysis by using a normalization of the selected eigenvectors. Therefore, the shape is defined, but not the absolute deformation. We will use the scaling of the eigenvectors to create the structure deformation for the dynamic analysis.

## 2.2 Buckling modes of the structure

This study considers a structure of square section (64 mm per side), fixed length (150 mm) and homogeneous thickness. This size was selected because it is a common one for the frontal rail and crash box of cars. The general study is presented considering the use of a mild steel to discuss the structure properties and later considering different thicknesses and materials, including both steel and aluminium, always keeping the same section size. All materials were implemented in the models according to their elasto-plastic properties using an isotropic hardening rule and applying the tangent module profile for the values in the range between yield to ultimate strength. The values of the properties of the different materials are listed in Table 1. The material selection was done considering that mild steels are widely used for energy absorbers (Baroutaji, 2017), so we considered the cases of S355 and S235 (EN 10025-2) and the lighter structural aluminium alloys (ENAW or AA 6060) (Baroutaji, 2017; Guillow, 2001; Reyes, 2002).

Table 1 - Values of the elasto-plastic properties of the materials used in the studies.

| | **steel S355** | **steel S235** | **aluminium AA6060 T4** | **aluminium AA6060 T6** |
|---|---|---|---|---|
| **Elastic Modulus [GPa]** | 210 | 210 | 70 | 70 |
| **Yield Strength [MPa]** | 355 | 235 | 90 | 215 |
| **Tangent Modulus [GPa]** | 1.30 | 1.10 | 0.56 | 0.50 |
| **Density [kg/m$^3$]** | 7850 | 7850 | 2700 | 2700 |
| **Poisson Coefficient** | 0.30 | 0.30 | 0.33 | 0.33 |

The study of the eigenvalue buckling analysis and mode shapes was done with the software package Ansys Mechanical (v18.2, Ansys, PA, USA). We analysed the initial 70 buckling modes for making a selection of the more convenient cases, considering both the efficient performance and the easy of a future application into a production process. The first selection option is for cases with the deformation affecting to all the faces, being more effective for load smoothing. Then we select the cases with deformations with a simple waving profile in each face section, either convex or concave, and removing not simple profile. The selected cases showed a different number of plies along the length of the structure. In Figure 1 there are plots of three buckling cases obtained for the geometry under study. The case on the left

panel shows a not-simple profile in some faces; the case on the central panel contains not deformed faces; the case of the right panel shows simple profiles in all faces. Only the later case would be a candidate according to our criteria.

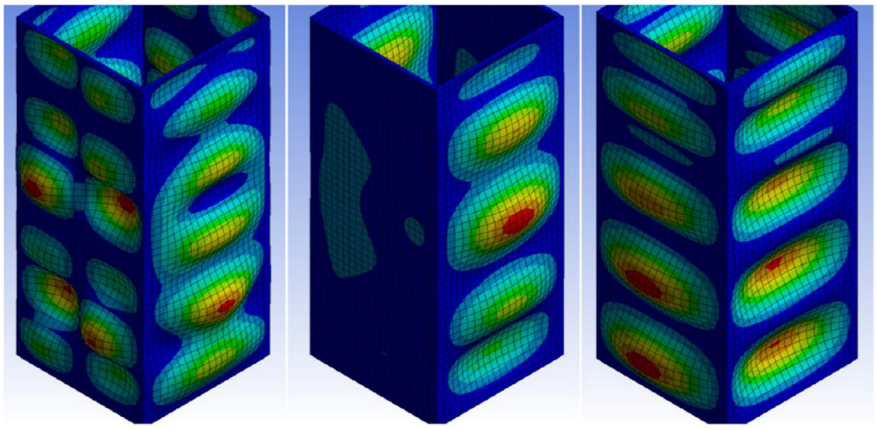

Fig. 1 - Drawing of different buckling cases obtained for the structure of this case study. We can observe that not-simple profiles (in a section) appear on the faces of the case on the left panel, and some face is not deformed for the case in the central panel. The case on the right panel shows simple profiles on each face.

For the final selection of modes to consider we opted for those with peak distances about 50 mm, inducing at least three plies in the folding pattern. In Figure 2 we plot the six different mode shapes corresponding to the selections applied to this case study. These modes correspond to the buckling described by Hirose [Hirose, 2014]. The author describes the mixed and independent modes, corresponding to cases that include concave and convex profiles in the same section (mixed mode), as for types 28, 37 and 53 in Figure 2; and cases that include either concave or convex profiles in the same section (independent mode), as for types 25, 30, 39 in Figure 2. In our study, the initial regular crash-box geometry will be pre-deformed according to the selected buckling shapes, and the dynamic study of the axial-crushing is done with these new geometry conditions.

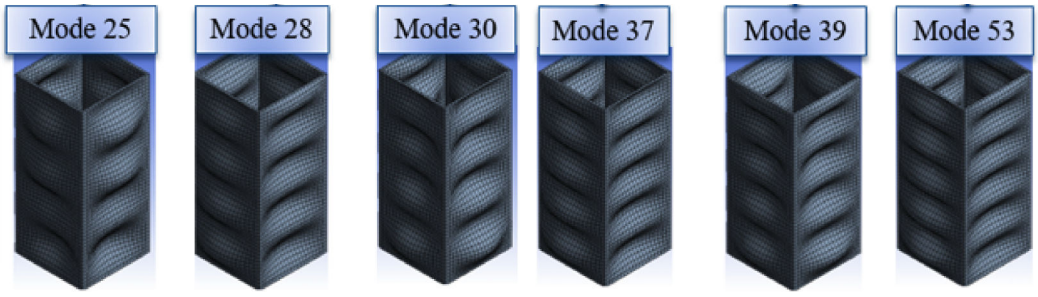


Fig. 2 - Drawings of the deformation patterns associated to the selected buckling mode shapes calculated for the structure of this case study. Some of the modes (28, 37, 53) include concave and convex profiles in the same cross section (mixed mode), while other modes (25, 30, 39) include either concave or convex profiles (independent mode).

## 3. DYNAMICAL TEST

The axial-crushing test was modelled considering the impact of an infinitely rigid surface against one open face of the structure, and perpendicular to the structure longitudinal axis. The impact conditions (mass and velocity of the impacting surface) were defined according to

the reference dissipation energy value 2.17 kJ, provided by 250 kg at 15 km/h. We used these values to establish a link with other works (Baykasoglu, 2015; Hou, 2011), and increased the speed to make full use of the structure capability. The nodes of the mesh at the opposite plane were defined a fixed.

We used the software package LS-DYNA (R8.1.0, Livermore Software Technology Corp. CA, USA) for the evaluation of the explicit FE model of the impact. The mode shapes obtained were redefined according a given scaling factor, and the modified mesh was used as the input data for the crushing test. The method of using the buckling mode shapes as input for the dynamic analysis was applied to cylindrical sections by (Shakery, 2007). However, the authors studied the input of imperfections in the mesh to mimic the real cases, while we are interested in true deformations for controlling the plastic buckling modes.

The mesh, structured, was defined with linear square (shell) elements. We performed a mesh size sensitivity analysis, studying cases with element sizes between 1 and 3 mm. The results did not change appreciably; the load profiles and maximum values were similar, the results provided loads slightly higher for higher sizes. However, the data generated increased by a factor 6 and the computing time increased largely (factor 41) in that range. Therefore, we set the element size to 3 mm. This element size is then appropriate to describe the mesh for both the studies, the static buckling of the structure and the dynamic behaviour under impact.

## 4. MODES AND DEFORMATION SCALING

The mode shapes associated to buckling were converted into actual deformations by scaling the mode amplitudes. The maximum displacement of each mode shape is set to 1 mm deformation and additionally a scaling factor is applied to the overall shape to define the total deformation for considering different options. The following study was done considering the material S355 and a box thickness of 1.6 mm.

In Figure 3 we plot the load time profile calculated during the axial crushing process. The line A corresponds to the original (un-deformed) geometry of the structure. In the initial 3 ms there are three load peaks corresponding to the formation of buckling plies of the structure, and reach values above 100 kN. Then the load decays passing through a long plateau between 10 and 22 ms., which corresponds to the crushing of the plies.

The other curves correspond to evaluations of the pre-deformed structures according to the (mixed) mode shape 28 and with scaling factors of x7 (line B), x10 (line C) and x13 (line D). In the initial 3 ms. we observe two peaks corresponding to the deformation after two plies start working. From that time the load decays until the next ply starts working at 10 ms, causing a soft and broad load peak. The maximum load peak caused by the original geometry (108 kN) is reduced more than 50% after including the pre-deformation shapes. Setting lower scaling values did not help to produce this important change in maximum load. Setting higher scaling values did not change notably the results, while its production would require more deformation and therefore implies a higher cost with a limited effect. We conclude that the range of scaling values considered (x7 to x13) is adequate for the following discussions. The amplitude of the oscillations between maximum and minimum values during the plying process is also reduced with increasing scaling factor values. The scaling x13 produces the flatter oscillations and a maximum load of 41 kN.

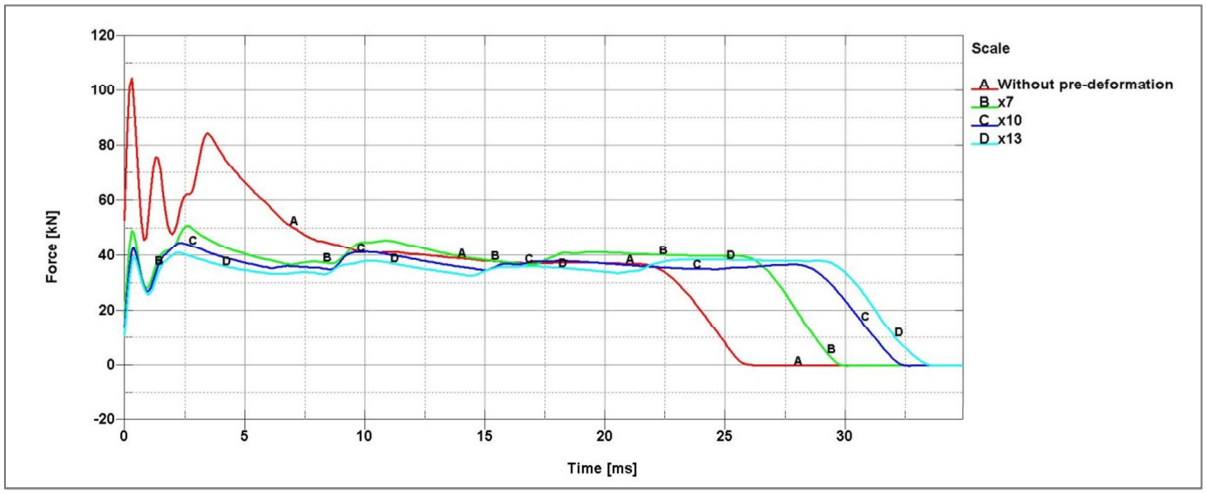


Fig. 3 - Load time profile calculated during the axial crushing process and corresponding to shape mode 28. The different curves correspond to the original geometry of the structure (A), and three different deformation scaling factors (B, C, D).

In Figure 4 we plot the results of the load time profile for the (independent) mode shape 39. We can observe that the different deformation scaling values produce different force profiles in the initial 20 ms after the impact. The mode with scaling x7 (line A) produces a maximum value of 59 kN, while setting scaling x13 (line C) does not cross above 50 kN. There are large differences of the load oscillations among the modes. At about 17 ms the loads converge to a similar value, and then the load decays the faster the smaller the initial deformation scaling is. The same behaviour of the tail of load is observed in the mixed mode 28 (cf. Figure 3). The final load flank at the end of the crushing process is ruled by the residual energy left after the plying of the structure. The faster the energy absorption (higher peaks), the earlier the load decays. Otherwise, a more progressive energy absorption induces also a longer crushing time, and the load decay happens later.

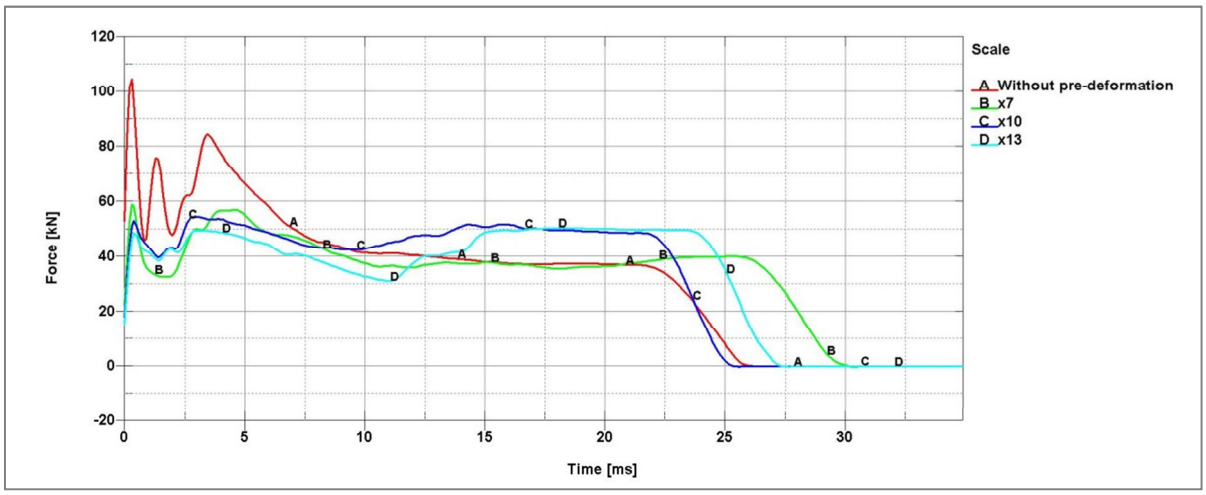


Fig. 4 - Load time profile calculated during the axial crushing process and corresponding to shape mode 39. The different curves (A, B, C) correspond to different scaling factors.

The mixed mode shapes (types 28, 37 and 53 in Figure 2) produced load patterns alike to mode 28, cf. Figure 3. In Figure 5 we plot the load time profile trough the axial crushing test for these modes, each mode with the more favourable scaling factor, considering the maximum load and the amplitude of load oscillations. The deformation patterns associated to

independent modes (labels 25, 30 and 39 in Figure 2) induced higher loads, that is, they are more resistant to deformation as found in (Hirose, 2014). Also the total amplitude of the oscillation between maximum and minimum values during the plying process was higher.

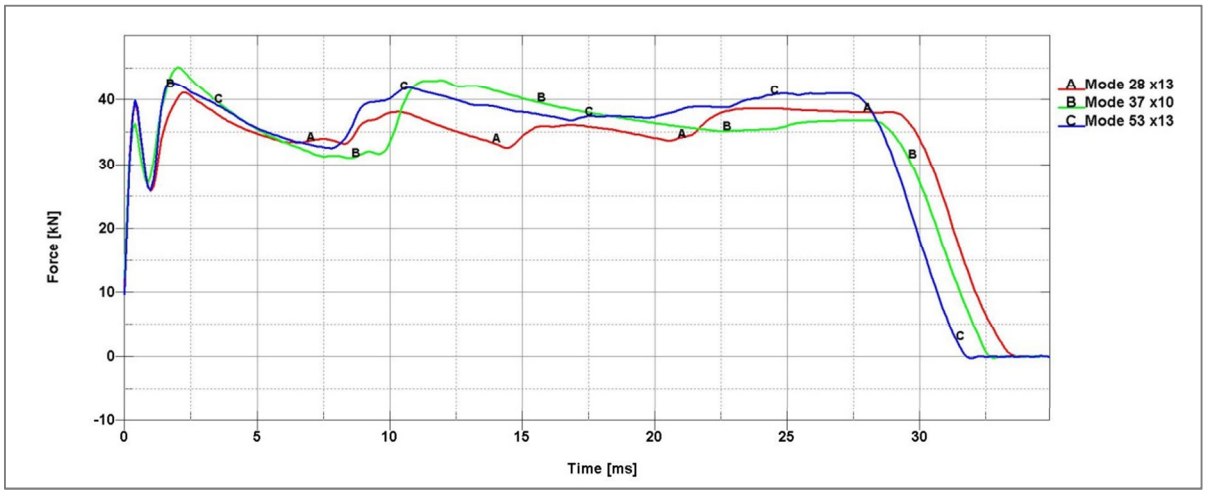


Fig. 5 - Load time profile calculated during the axial crushing process and corresponding to shape modes 28 (scaling x13, line A), 37 (scaling x10, line B) and 53 (scaling x13, line C).

Clearly the load patterns are ruled by the mode type, either mixed or independent. The scaling may be tuned to produce similar load profiles for each mode type. According to these results, the best performance is achieved by mode 28 and a scaling x13. This option reduces more than 60% de maximum peak load in respect to the initial geometry, and the amplitude of the oscillation is reduced to few kN. around the level of 35 kN.

## 5. WALL THICKNESS INFLUENCE

We can discuss the effect of the wall thickness studying and comparing the same selected case (mode shape 28 with scaling factor x13, for S355 steel). It is important to note in pass that the change of thickness does not influence the mode shapes associated to the structure. It would simply modify the relation between the applied charge and the critical buckling load.

In Figure 6 we plot the load time profile during the impact, analysing the results for the thicknesses values 1.6 (line A), 1.4 (B) and 1.3 mm (C) of steel S355. The lower the thickness, the lower the plying resistance and also the load peaks appearing in the crushing test, although the whole process increases its time spam. In the initial 30 ms, the (maximum) load peak value changes 34%, from 41 kN (1.6 mm) to 27 kN (1.3 mm). The amplitude of oscillations rather similar, about 5 kN in multiple bumps.

We can observe that all cases show a broad peak at the last third of the crushing process, being more pronounced at the 1.3 mm case (line C) increasing about 27%. At the end of the plying process, the structure cannot take more energy and the compression increases. The lowest thickness (line B) is the preferable case: lower maximum load values, lower load average and similar load oscillation.

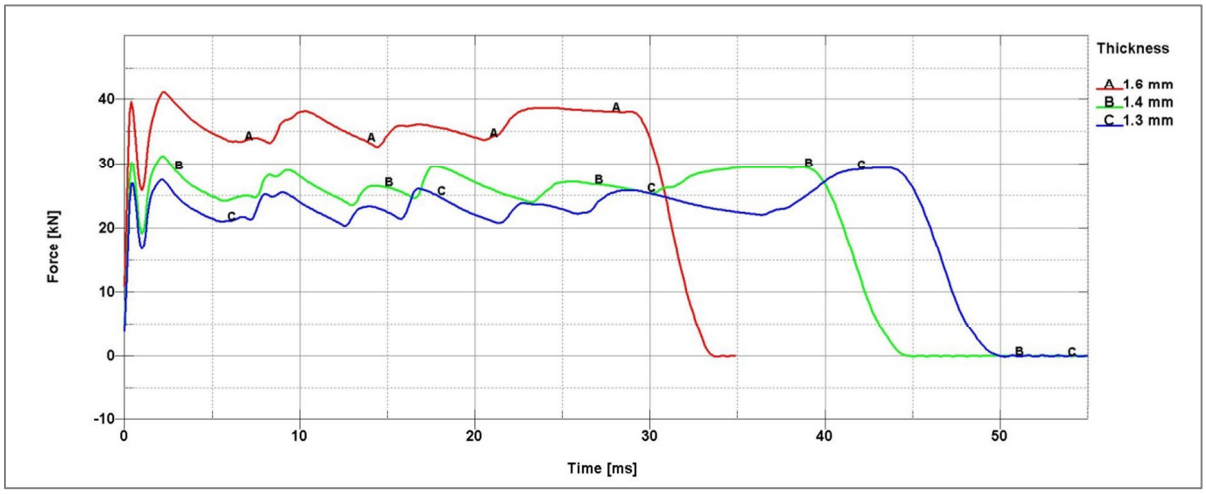


Fig. 6 - Load time profile calculated during the axial crushing process and corresponding to the shape mode 28 (scaling x13), considering the same material (steel S355) and for different wall thicknesses: 1.6 mm (A), 1.4 mm (B) and 1.3 mm (C).

## 6. MATERIAL INFLUENCE

After analysing the most convenient initial geometry to produce a smooth load pattern under crushing, the analysis focuses now in the influence of the material selected for the structure. We considered the same buckling mode (28) and scaling (x13) for the study. The wall thickness for each material case was adapted to produce results comparable in maximum load value and a soft load oscillation in the crushing process. Therefore, the different options will produce a similar solution for dissipating the same energy, while the material and process cost, as well as the weight of the structure, would be different.

The convenient thicknesses for each material were analysed and the final values defined according the load profiles observed: 1.4 mm for S355, 1.6 mm for S235, 2.0 mm for AA6060-T6 and 2.6 mm for AA6060-T4. The specific energy absorption values obtained in this study are listed in Table 2, corresponding to the well-known behaviour of higher stiffness and lower masses favouring higher coefficients. For the same material the higher yield strength allows for a lower structure mass to produce equivalent energy absorption, as scaled with the absorption coefficient.

Table 2 - Values obtained for energy absorption for the materials used in this study.

| | **Steel S355** | **Steel S235** | **Aluminium AA6060 T4** | **Aluminium AA6060 T6** |
|---|---|---|---|---|
| **Energy Absorption [kJ/kg]** | 4,492 | 3,931 | 6,961 | 8,991 |

In Figure 7 we plot the load time profile during the crushing process for the different steel and aluminium materials (cf. Table 1), with the appropriate thicknesses. The plying pattern rules completely the load profile. All materials show two load peaks in the initial 7 ms. The higher values correspond to steel S355 and aluminium AA6060-T6, with a similar profile and peak values for most of the time spam. All materials absorb the energy along a similar time spam, taking advantage of the plying geometry, and increasing the load just at the end of the

deformation process when the contact between plies is predominant. The cases of the softer materials show a fast plying: steel S235 shows one more peak at 12 ms, missing in aluminium AA6060-T4, and a continuous load increase after 15 ms to reach the maximum load at the end of the time spam.

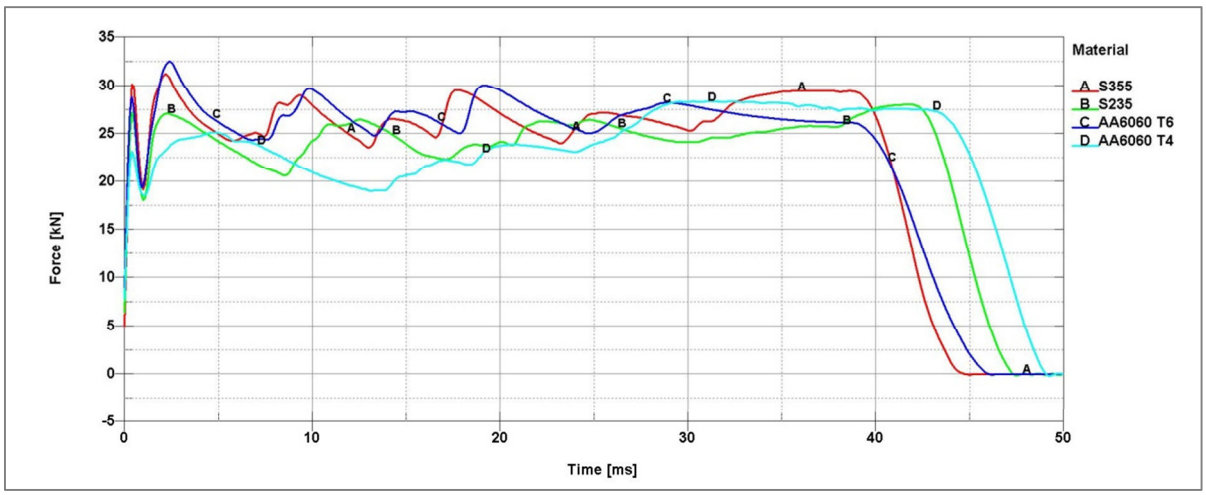


Fig. 7 - Load time profile calculated during the axial crushing process and corresponding to shape mode 28 (scaling x13), considering different materials. The wall thicknesses were adapted in each case to produce similar load maximum peaks and soft load oscillations.

## 7. THE COUPLING OF THE CRASH-BOX IN A BUMPER SYSTEM

The selection of an optimum crash-box is possible according with the previous discussions. We analyse now the performance of a bumper coupled to the selected crash-box. The bumper system includes the bumper and two lines of crash-boxes located symmetrically at each side, being part of the front-rail group, see Figure 8, upper panel. The study was done considering an impact against a rigid wall normal to the bumper. The impact values considered were 15 km/h and a mass of 500 Kg (4.34kJ), being almost equivalent to the single crash-box case analysed above due to the symmetry of the system. The shape of the bumper (2.5 mm thick) was taken from a commercial vehicle, but the details are not of interest in this discussion. The mesh of the boxes and bumper were the same type, with sizes of 3 mm and 5 mm respectively. The material used in this study was S235 and thickness of 1.6 mm for the crash-box. In Figure 8 the drawings show a detail of the assembly of the bumper and one pre-deformed crash-box at different moments during the impact.

In Figure 9 we plot the load time profile during the impact into the bumper and crash-box coupled system measured at one crash-box. The two lines correspond to the coupling of the original crash-box (constant regular section) and the modified crash-box (according the mode 28 and scaling x13). The load profiles are similar the initial 10 ms, due to the fact that the bumper makes mostly the energy absorption: its low rigidity induces the low load values. Then the deformation of the crash-box increases fast. And thereafter the load curves differ largely dominated by the crash-box performance. The narrow high peaks of the original crash-box (cf. Figure 3) build a large load peak in the system in a short time (20 ms), and the load decreases till the end. The modified crash-box makes the expected work, causing smoothed load peaks, with rather low oscillation and broad and limited peaks till the end.

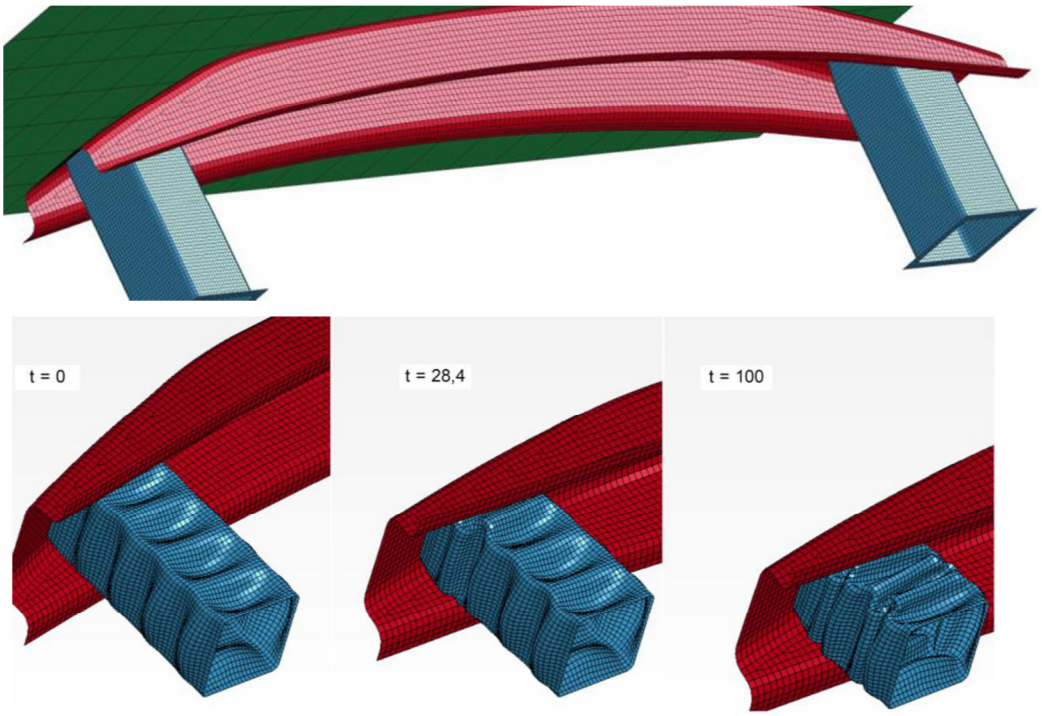


Fig. 8 - Bumper system. Upper panel: the bumper is fixed with two crash-boxes located symmetrically. The axial impact (rigid wall) is normal to the bumper. Lower panels: Detail of the assembly of a bumper and the crash-box at different time frames during the crushing process after an axial impact.

Comparing the load profile between the crushing of the crash-box (Figure 7) and the assembly of crash-box and bumper (Figure 9) we found that with the same material and thickness (S235 1.6 mm) the average force is higher when the crash-box works alone (22-26 kN) than working coupled (19-25 kN). This behaviour is solely due to the difference between the simple axial load of the first case and the added bending effect caused by the bumper in the coupled system.

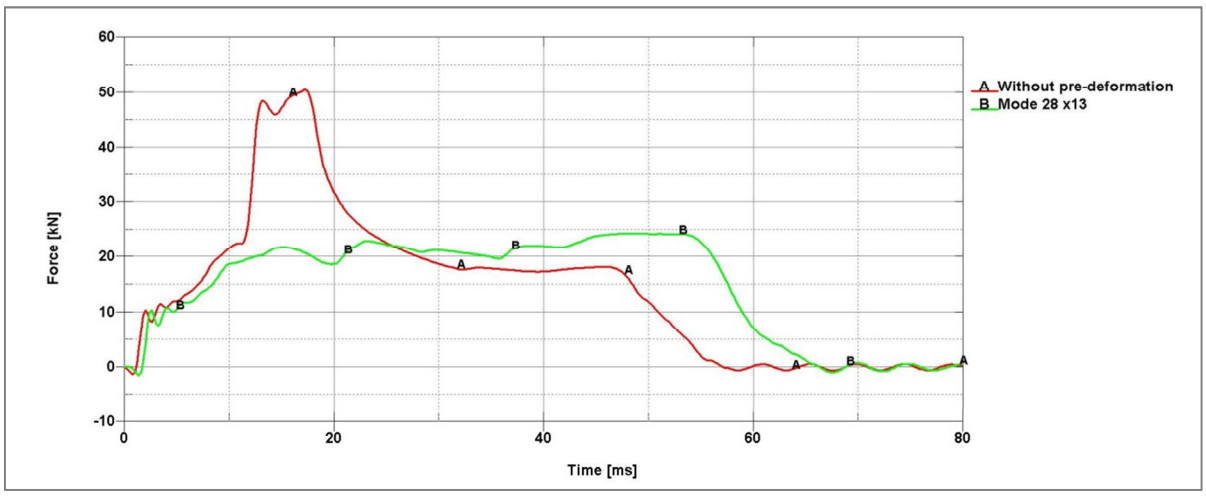


Fig. 9 - Load time profile calculated during the axial crushing process of the bumper coupled to the crash-box. The lines correspond to the original (uniform section) crash-box (line A), and to the selected pre-deformed crash-box (line B).

## 7.1 SERIAL CRASH-BOX MOUNTING

The possibility to track and design the load profile through the crash-box deformation allows for proposing and analysing different configurations to improve the energy absorption capabilities of a system.

Two crash-boxes mounted in series can be designed so that one box with lower critic load starts crushing initially at impact conditions. After its crushing limit, the second box stars its own crushing, see Figure 10. The dynamic simulation shows that the two boxes may work in a sequential process as described. The crash-box system is dedicated to the typical situation of low velocity impact, set at 15 km/h (RCAR or AZT tests). Therefore we can consider a design so that under a certain limit of energy one crash-box is used, while the second one remains un-touch. At higher energies, both boxes would be crushed.

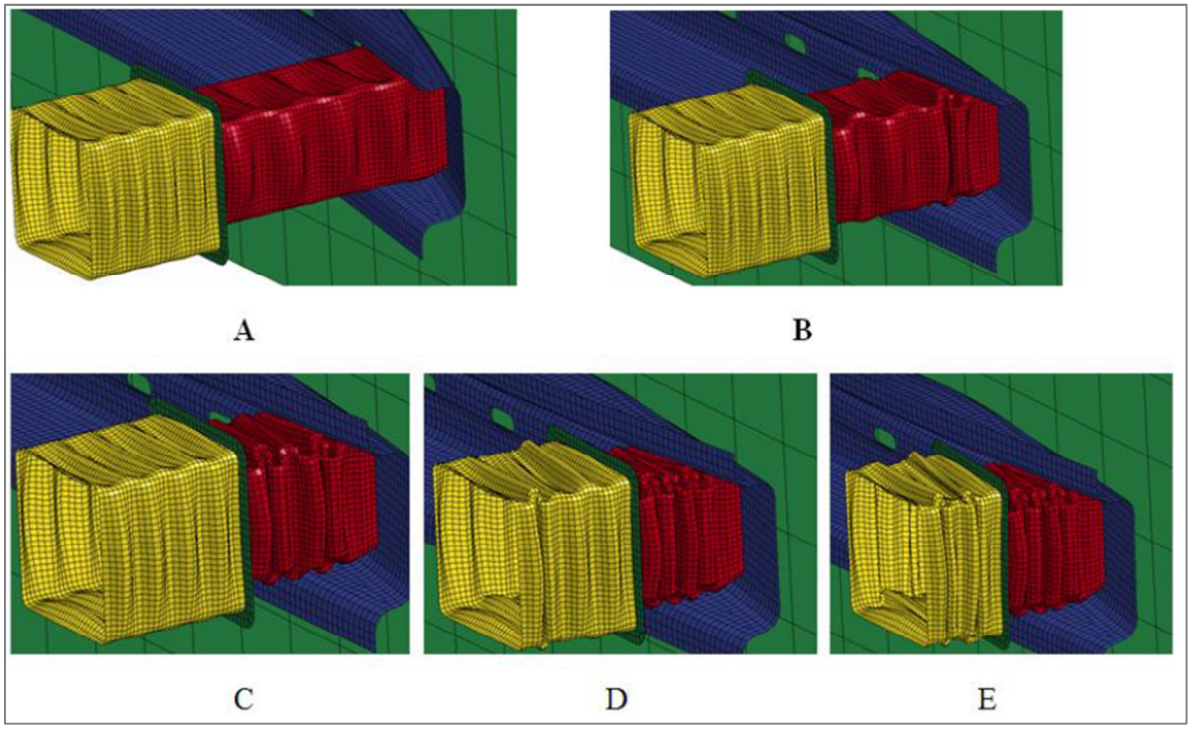


Fig. 10 - Drawings of two serial crash-boxes coupled with a bumper in several time frames during an axial crushing. The weaker box starts plying and the increase of load at the end of its plying causes the deformation of the second box.

To study this case we analysed and compared an impact performed at 15 km/h against a 500 kg wall (4.34 kJ), and a case with 78% extra energy (20 km/h, 7.72 kJ). The two crash-boxes were set in series, one with the same size as the previously studied case and 1.6 mm thickness, and a second one scaled in section to 84 mm edge and 1.6 mm thickness. Both boxes were made of steel S235 pre-deformed according to the appropriate buckling shape mode and scaling factor as described before. The parts were joined together by a simple plate (5 mm

thick) in between. The total length was 235 mm, short enough to be realistic in the usual compact available space.

The mesh of the boxes and bumper were the same type and size as before. The plate was defined with the same elements of 4 mm size. The results calculated for the load time profile are plot in Figure 11 for 20 km/h (line A) and 15 km/h (line B). The loads correspond to one line of crash boxes, not to the total of the bumper system. For comparison we also plot the load profile of the crash-box working alone with 15 km/h (1.6 mm thickness, Figure 7). For the serial mounting we can distinguish three regions. In the region just after the impact (0-5 ms) the compliant bumper makes the most of the energy absorption, causing low load values. In the second region (5-25 ms), the first crash-box plies and the load reaches a rather constant level about 22 kN. The behaviour is rather similar for both velocities (lines A and B) because it is only the first crash-box that absorbs the energy. In the last region, at 15 km/h (line B) the load increases smoothly to 24 kN and decays. At 20 km/h (line A) the second box plies and the load increases up to 35 kN. A more elaborated design (reducing the thickness of the second box) could decrease and smooth that profile. Here we wanted to show the sequential action of the serial setup.

With increasing energies, the load patterns are rather similar in regions 1 and 2, and they differ only in the third region. This shows that the first crash-box makes completely its work before the second box starts working. This characteristic of the serial mounting allows for designing systems where one part may preserve its integrity for impacts up to a certain energy level. This concept helps in the modularity of the safety systems.

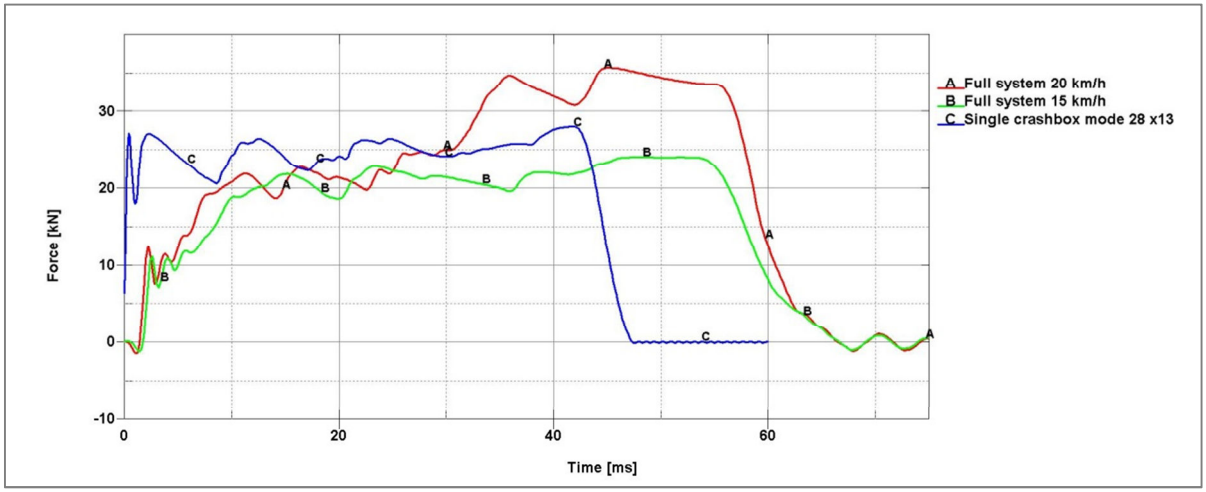


Fig. 11 - Load time profile calculated during the axial crushing process of a bumper coupled to a double crash-box in series. The results correspond 20 km/h (line A) and 15 km/h (line B). The profile for a single crash box and 15 km/h is also plot (line C).

## 8. CONCLUSIONS

The front-rail of the vehicles is a key system for the energy absorption performance during an impact situation. The crash boxes are mechanical parts whose deformation influences notably the load pattern transmitted through the whole structure, specially designed for low-speed impact situations.

In this work we have studied the design of a crash box to produce a characteristic load pattern smoothing off the peaks and causing low load oscillations. We have used the analysis of the buckling mode shapes to select a collection of preferred candidates. The criteria were based both in the efficiency for tuning the load patterns and the feasibility for industrial application. The structures were pre-deformed according the mode shapes, and then studied under impact. The analysis and comparison of the loads induced by this set of modes allowed for selecting the best performance options. We focused in using a squared section, and set a size for making the analysis. We found that the pre-deformed structures caused a 60% reduction of the peak loads induced by a uniform section structure. Also the load oscillations were very much reduced, to some 5 kN (amplitude). We also analysed the influence of the wall thickness in the load patterns. The studies included a few typical materials (steels and aluminium alloys) for comparison of the influence of different rigidities and strengths.

The possibility to select a preferred crash box by using the proposed method also opens the opportunity to study the effect of coupling the box into a bumper system. In real conditions there are typically no simple axial impacts, therefore we have used comparable loads. We have analysed how the load pattern of the whole system responds rather well according to the box-induced load pattern. We proposed to couple the crash boxes in series to further control by design the load pattern in cases with increased energy. We found that the boxes set in series allows for splitting the deformation in independent stages limited by energy levels. This method may be implemented to have a better control on the level of damage caused in low speed impacts.

## ACKNOWLEDGMENTS

The work of J.R. Fernández was partially supported by the Ministerio de Economía y Competitividad (Spain) under the research project MTM2015-66640-P (with FEDER Funds).

E. Casarejos, J.A. López-Campos, A. Segade and J.A. Vilán gratefully acknowledge the funding by Xunta de Galicia (Spain) under the program ‘Grupos de Referencia Competitiva’, with Ref. GRC2015/016.

J.A. López-Campos also acknowledges the funding from the Xunta de Galicia (Spain) under the program ‘Axudas de apoio a etapa predoutoral’, with Ref. ED481A-2017/045.

## REFERENCES

[1] Abramowicz W, Jones N. Dynamic axial crushing of square tubes. International Journal of Impact Engineering, 1984, 2, pp. 179-208.

[2] Abramowicz W, Jones N. Dynamic axial crushing of circular tubes. International Journal of Impact Engineering, 1984, 3, pp. 263-281.

[3] Abramowicz W, Jones N. Dynamic progressive buckling of circular and square tubes. International Journal of Impact Engineering, 1986, 4, pp. 243-270.

[4] Abramowicz W, Jones N. Transition from initial global bending to progressive buckling of tubes loaded statically and dynamically. International Journal of Impact Engineering, 1997, 19 (5-6), pp. 415-437.

[5] Acar E, Guler MA, Gerceker B, Cerit ME, Bayram B. Multi-objective crashworthinesss optimization of tapered thin-walled tubes with axisymmetric indentations. Thin-Walled Structures, 2011, 49, p. 94-105.

[6] Albert PC, Ghani ARA., Othman MZ, Zaidi AMAZ. Axial crushing behaviour of aluminium square tube with origami pattern. Modern Applied Science, 2016, 10 (2), pp. 90-108.

[7] Arnold B, Altenhof W. Experimental observations on the crush characteristics of AA6061T4 and T6 structural square tubes with and without circular discontinuities. International Journal of Crashworthiness, 2004, 9 (1), pp. 73-87.

[8] Asanjarania A, Dibajianb SH, Mahdiana A. Multi-objective crashworthiness optimization of tapered thin-walled square tubes with indentations. Thin-Walled Structures, 2017, 116, pp. 26-36.

[9] Baykasoglu C, Cetin MT. Energy absorption of circular aluminium tubes with functionally graded thickness under axial impact loading. International Journal of Crashworthiness, 2015, 20 (1), pp. 95-106.

[10] Cook RD, Malkus DS, Plesha ME, Witt RJ. Concepts and applications of finite element analysis. Ed. Wiley, 1974, pp. 429-454.

[11] Davies GAO, Morton J. Structural impact and crashworthiness. Elsevier Applied Science Publishers, New York, 1984.

[12] Guillow SR, Lu G, Grzebieta RH. Quasi-static axial compression of thin-walled circular aluminium tubes. International Journal of Mechanical Sciences. 2001, 43 (9), pp. 2103-2123.

[13] Grzebieta RH, Murray NW. The static behaviour of struts with initial kinks at their center points. International Journal of Impact Engineering, 1985, 3 (3), pp. 155-65.

[14] Grzebieta RH, Murray NW Energy absorption of an initially imperfect strut subjected to an impact load. International Journal of Impact Engineering, 1986, 4 (3), pp. 147-59.

[15] Hirose S. Shock absorbing member PCT No.: PCT/JP2012/070109 Feb.7, 2014.

[16] Hosseinipour SJ, Daneshi GH. Energy absorption and mean crushing load of thin-walled grooved tubes under axial compression. Thin-Walled Structures, 2003, 41 (1), pp. 31-46.

[17] Hou S, Han X, Sun G, Long S, Li W, Yang X, Li Q. Multiobjective optimization for tapered circular tubes. Thin-Walled Structures, 2011, 49, pp. 855-863.

[18] Kokkula S, Langseth M, Hopperstad OS, Lademo OG. Offset impact behaviour of bumper beam-longitudinal systems: experimental investigations, International Journal of Crashworthiness, 2006, 11 (4), pp. 299-316.

[19] Kokkula S, Hopperstad OS, Lademo OG, Berstad T, Langseth M. Offset impact behaviour of bumper beam-longitudinal systems: numerical simulations, International Journal of Crashworthiness, 2006, 11 (4), pp. 317-336.

[20] Langseth M, Hopperstad OS, Berstad T. Crashworthiness of aluminium extrusions: validation of numerical simulation, effect of mass ratio and impact velocity. International Journal of Impact Engineering, 1999, 22, pp. 829-854.

[21] Langseth M, Berstad T, Hopperstad OS, Clausen AH. Energy Absorption in Axially Loaded Square Thin-Walled Aluminium Extrusions. Transactions on the Built Environment, 1994, 8, pp. 401-410.

[22] Lee S, Hahn C, Rhee M, Oh J. Effect of triggering on the energy absorption capacity of axially compressed aluminium tubes. Materials & Design, 1999, 20, pp. 31-40.

[23] López-Campos JA, Segade A, Vilán JA, García-Nieto PJ, Blanco J. Study of a Steel's Energy Absorption System for Heavy Quadricycles and Nonlinear Explicit Dynamic Analysis of its Behavior under Impact by FEM. Materials, 2015, 8 (10), pp. 6893-6908.

[24] Karagiozova D, Norman J. On dynamic buckling phenomena in axially loaded elastic-plastic cylindrical shells. International Journal of Non-Linear Mechanics, 2002, 37, pp. 1223-1238.

[25] Mamalis AG, Manolakos DE, Viegelhan GL, Johnson W. Energy absorption and deformation modes of thin PVC tubes internally grooved when subjected to axial plastic collapse. In: Proceedings of the Institution of Mechanical Engineers, 1989, 203, pp. 1-8.

[26] Mamalis AG, Manolakos DE, Spentzas KN, Ioannidis MB, Koutroubakis S, Kostazos PK. The effect of the implementation of circular holes as crush initiators to the crushing characteristics of mild steel square tubes: experimental and numerical simulation. International Journal of Crashworthiness, 2009, 14 (5), pp. 489-501.

[27] Nagel GM, Thambiratnam DP. Dynamic simulation and energy absorption of tapered thin-walled tubes under oblique impact loading. International Journal of Impact Engineering, 2006, 32, pp. 1595-1620.

[28] Reyes A, Langseth M, Hopperstad OS. Crashworthiness of aluminum extrusions subjected to oblique loading: experiments and numerical analyses. International Journal of Mechanical Sciences, 2002, 44 (9), pp. 1965-1984.

[29] Shakeri M, Mirzaeifar R, Salehghaffari S. New insights into the collapsing of cylindrical thin-walled tubes under axial impact load. Proceedings of the Institution of Mechanical Engineers, Part C: Journal of Mechanical Engineering Science, 2007, 221 (8), pp. 869-885.

[30] Tanlak N, Sonmez FO, Senaltun M. Shape optimization of bumper beams under high-velocity impact loads. Engineering Structures, 2015, 95, pp. 49-60.

[31] Tanlak N, Sonmez FO, Senaltun M. Optimal shape design of thin-walled tubes under high-velocity axial impact loads. Thin-Walled Structures, 2014, 84, pp. 302-312.

[32] Witteman WJ. Improved Vehicle Crashworthiness Design by Control of the Energy Absorption for Different Collision Situations. Ph.D. Thesis, Eindhoven University of Technology, Eindhoven, The Netherlands, 15 June 1999.

[33] Yamazaki K, Han J. Maximization of the crushing energy absorption of tubes. Structural Optimization, 1998, 16, pp. 37-46.

[34 Yuen SCK, Nurick GN. The energy-absorbing characteristics of tubular structures with geometric and material modifications: an overview. Applied Mechanics Reviews, 2008, 61 (2), pp. 20802 1-15.